

A HARPS RV search for planets around young nearby stars

A. Grandjean¹, A.-M. Lagrange¹, M. Keppler², N. Meunier¹, L. Mignon¹, S. Borgniet³, G. Chauvin¹, S. Desidera⁴, F. Galland¹, S. Messina⁵, M. Sterzik⁶, B. Pantoja⁷, L. Rodet¹, and N. Zicher⁸

¹ Univ. Grenoble Alpes, CNRS, IPAG, 38000 Grenoble, France

e-mail: Antoine.Grandjean1@univ-grenoble-alpes.fr

² Max Planck Institute for Astronomy, Königstuhl 17, D-69117 Heidelberg, Germany

³ CNRS Lesia (UMR8109) - Observatoire de Paris, Paris, France

⁴ INAF-Osservatorio Astronomico di Padova, Vicolo dell'Osservatorio 5, Padova, Italy, 35122-I

⁵ INAF-Osservatorio Astrofisico di Catania, via Santa Sofia, 78 Catania, Italy

⁶ European Southern Observatory (ESO), Alonso de Córdova 3107, Vitacura, Casilla 19001, Santiago, Chile

⁷ Departamento de Astronomía, Universidad de Chile, Camino al Observatorio, Cerro Calán, Santiago, Chile

⁸ Oxford Astrophysics, Department of Physics, Denys Wilkinson Building, UK

Received 2019 June 11/ Accepted 2019 October 14

ABSTRACT

Context. Young nearby stars are good candidates in the search for planets with both radial velocity (RV) and direct imaging techniques. This, in turn, allows for the computation of the giant planet occurrence rates at all separations. The RV search around young stars is a challenge as they are generally faster rotators than older stars of similar spectral types and they exhibit signatures of magnetic activity (spots) or pulsation in their RV time series. Specific analyses are necessary to characterize, and possibly correct for, this activity.

Aims. Our aim is to search for planets around young nearby stars and to estimate the giant planet (GP) occurrence rates for periods up to 1000 days.

Methods. We used the HARPS spectrograph on the 3.6 m telescope at La Silla Observatory to observe 89 $A - M$ young (< 600 Myr) stars. We used our SAFIR (Spectroscopic data via Analysis of the Fourier Interspectrum Radial velocities) software to compute the RV and other spectroscopic observables. Then, we computed the companion occurrence rates on this sample.

Results. We confirm the binary nature of HD177171, HD181321 and HD186704. We report the detection of a close low mass stellar companion for HIP36985. No planetary companion was detected. We obtain upper limits on the GP ($< 13 M_{\text{Jup}}$) and BD ($\in [13; 80] M_{\text{Jup}}$) occurrence rates based on 83 young stars for periods less than 1000 days, which are set, 2_{-2}^{+3} % and 1_{-1}^{+3} %.

Key words. Techniques: radial velocities – stars: activity – (stars:) binaries: spectroscopic – stars: planetary systems – stars: starspots – stars: variables: general

1. Introduction

More than four thousand exoplanets have been confirmed and most of them have been found by transit or radial velocity (RV) techniques^a. The latter, although very powerful, is limited by the parent star's activity (spots, plages, convection, and pulsations). Young stars are generally faster rotators than their older counterparts (Stauffer et al. 2016; Rebull et al. 2016; Gallet & Bouvier 2015). They can also exhibit activity-induced RV jitter with amplitudes up to 1 km s^{-1} (Lagrange et al. 2013), larger than the planet's induced signal. False positive detections have been reported around young stars in the past (Huélamo et al. 2008; Figueira et al. 2010; Soto et al. 2015).

We have carried out an RV survey to search for planets around such young stars with the High Accuracy Radial velocity Planet Searcher (HARPS) (Mayor et al. 2003) and SOPHIE (Bouchy & Sophie Team 2006) spectrographs with the final aim of coupling RV data with direct imaging (DI) data, which will allow for the computation of detection limits, for each targets at all separations and then to

compute occurrences rates for all separations. A feasibility study was carried out by Lagrange et al. (2013) on 26 stars of the survey with HARPS, demonstrating that we can probe for giant planets (1 to $13 M_{\text{Jup}}$, hereafter GP) with semi-major axis up to 2 au and couple the survey data with direct imaging data. The time baseline of our survey also permits a probe of the hot Jupiter (Hereafter HJ) domain around young stars. Although GP formation models predict a formation at a few au (Pollack et al. 1996), migration through disc-planet interaction (Kley & Nelson 2012) or gravitational interaction with a third body can allow the planet to finally orbit close to the star (Teyssandier et al. 2019). HJ are common among exoplanets orbiting older main sequence stars as they represent one detected planet out of five (Wright et al. 2012). While previous RV surveys on small sets of young stars showed no evidence for the presence of young HJ (Esposito et al. 2006; Paulson & Yelda 2006), two HJ around young stars were recently discovered by Donati et al. (2016) and Yu et al. (2017). However, we still need to find out if this kind of object is common at young age or not and we need to compare the

^a exoplanet.eu

migration models with observations in order to constrain the migration timescales.

Here, we report on the results of our large HARPS survey. We describe our survey sample and observations in Section 2. In Section 3, we focus on GP, brown dwarf (BD), and stellar companions detections. In Section 4, we perform a statistical analysis of our sample and compute the close GP and BD occurrence rates around young stars. We conclude our findings in Section 5.

2. Description of the survey

2.1. Sample

We selected a sample of 89 stars, chosen to their brightness ($V < 10$), ages as found in the literature (< 300 Myr for most of them, see Table A.1), and distance (< 80 pc) determined from their HIPPARCOS parallaxes (van Leeuwen 2007). These criteria ensure we will get the best detection limits for both the HARPS RV and SPHERE DI surveys at, respectively, short (typically 2 – 5 au), and large (further than typically 5 au) separations. Indeed, observing bright stars allow us to obtain spectra with a better signal to noise ratio (S/N). Moreover, young planets are still warm from their formation and are then brighter, which lowers the contrast between them and their host stars, while short distances allow for better angular resolutions in direct imaging. Most of the targets are part of the SPHERE GTO The SpHERE Infrared survey for Exoplanets (SHINE) survey sample (Chauvin et al. 2017a). Binary stars with an angular separation on the sky that is lower than 2 arcsec were not selected to avoid contamination in the spectra from the companion.

Their spectral types range from A0V to M5V (Figure 1). Their projected rotational velocity ($v \sin i$) range from 0.5 to 300 km s^{-1} with a median of 11 km s^{-1} , their V-band magnitude are mainly between 4 and 10 with a median of 7.8. Their masses are between 0.6 and $2.74 M_{\odot}$ with median of $1.07 M_{\odot}$. Our sample includes 26 targets between A0 and F5V ($B - V \in [-0.05 : 0.52]$), 55 between F6 and K5 ($B - V \in [-0.05 : 0.52]$), and 8 between K6 and M5 ($B - V \geq 1.33$). Noticeably, our sample includes stars with imaged planetary or substellar companions (among them β Pic, AB Pic, HN Peg, GJ 504, HR8799, HD95086, HD106906 or PZ Tel). We present the main characteristics of our star sample in Figure 1 and Table A.1.

2.2. Observations

We observed our 89 targets mainly between 2013 and 2016. Some stars were part of previous surveys by Borgniet et al. (2017) and Lagrange et al. (2009a), which allows us to reach a time baseline up to 10 yr. Some stars had already been observed with HARPS before, some since the HARPS commissioning in 2003. Additional observations were also obtained in October 2017, December 2017, and March 2018.

We use the observing strategy described in Borgniet et al. (2017), which consist of recording two spectra per visit and to observe each target on several consecutive nights to have a good sampling of the short-term jitter. The median time baseline is 1639 days (mean time baseline of 2324 days), with a median number of spectra per target of 25 (52 on average) spaced on a median number of

12 nights (17 on average, Figure 2). Details can be found in Table A.1.

2.3. Observables

From the HARPS spectra we derived the RV and whenever possible the cross-correlation function (CCF), bisector velocity span (hereafter BVS), and $\log R'_{\text{HK}}$ with our SAFIR software for Spectroscopic data via Analysis of the Fourier Interspectrum Radial velocities. It builds a reference spectrum from the median of all spectra available on a given star and computes the relative RV in the Fourier plane. The computed RV are then relative to the reference spectrum. The efficiency of this method was proved in the search of companions (Galland et al. 2005b,a). We mainly use the correlation between RV and BVS to determine the main source of RV variability : magnetic activity, pulsations or companions (Lagrange et al. 2009a; Borgniet et al. 2017). We excluded spectra with S/N at 550 nm which was too high (> 380), to avoid saturation or too low (< 80), to avoid bad data, as well as spectra with an air mass that was too high ($\sec z > 3$), and spectra that were too different from the reference spectrum of the star ($\chi^2 > 10$). For M-type stars, we used a lower limit of 40 in S/N at 550 nm as it is a better compromise for these stars to provide enough spectra to perform our analysis without including bad spectra.

3. Detected companions in the HARPS survey

3.1. Long period companions, RV long-term trends, and stellar binaries

In this section we describe the stars for which we identified a GP companion with a period higher than 1000 days, a long-term trend RV signal or a binary signal. When possible, we characterize the companion using the *yorbit* software that fits RV with a sum of keplerian or a sum of keplerians plus a drift (Ségransan et al. 2011).

3.1.1. HD39060

β Pic is an A6V pulsating star that hosts an imaged edge-on debris (Smith & Terrile 1984) and gas disk (Hobbs et al. 1985), and an imaged GP at 9 au (Lagrange et al. 2009b, 2019a). This star presents also exocomets signatures in its spectra (Lagrange-Henri et al. 1988; Beust et al. 1989; Kiefer et al. 2014). β Pic was observed with HARPS since its commissioning in 2003, totalizing more than 6000 spectra with a mean S/N at 550 nm of 273. Until 2008, spectra were taken to study the Ca II absorption lines associated to the falling exocomets. Since 2008, we adopted a specific observation strategy, to properly sample the stellar pulsations and to correct the RV from them, (Lagrange et al. 2012, 2019b). It consisted in observing the star for continuous sequences of 1 – 2 h. Longer sequences up to 6 h were obtained in 2017 – 2018. This allowed to detect a new GP companion within the pulsations signal of β Pic. The discovery of this $10 M_{\text{Jup}}$, 1200 days period companion is detailed in Lagrange et al. (2019b).

3.1.2. HD106906

HD106906 is a F5V star in the Sco-Cen young association. Bailey et al. (2014) Imaged a giant planet companion at

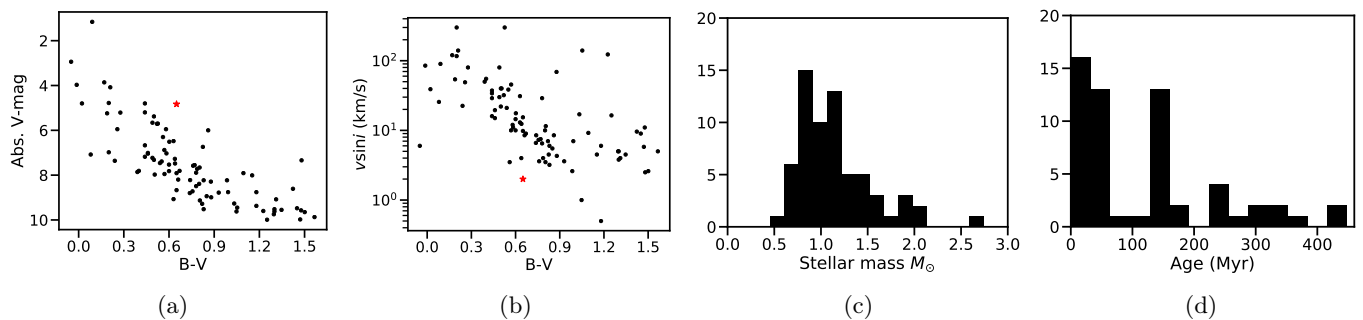


Fig. 1: Main physical properties of our sample. a) Absolute V -magnitude vs $B - V$. Each black dot corresponds to one target. The Sun is displayed (red star) for comparison. b) $v \sin i$ vs $B - V$ distribution. c) Mass histogram (in M_{\odot}). d) Age histogram.

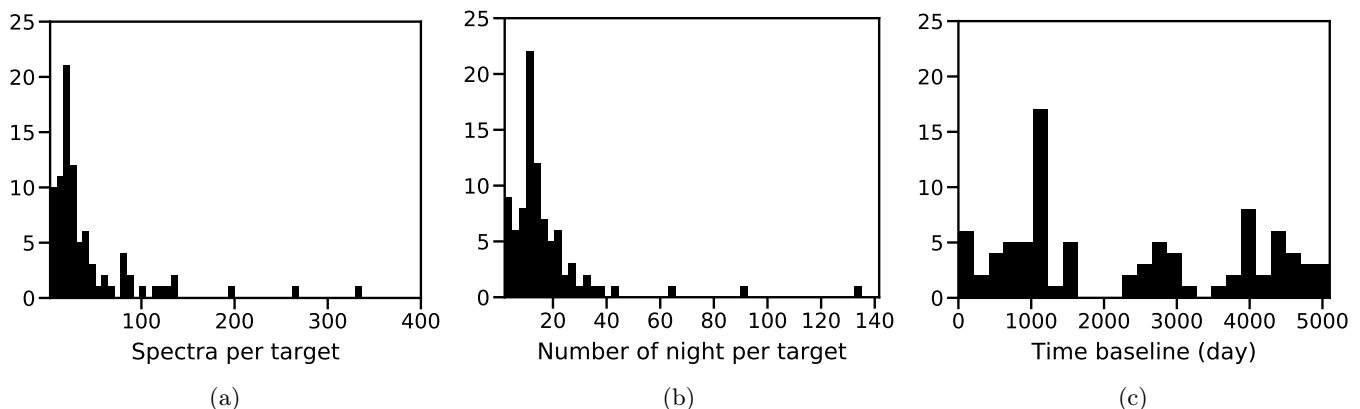


Fig. 2: Observation summary. a) Histogram of the number of spectra per target, excluding HD216956 (Fomalhaut, 834 spectra) and HD039060 (β Pic, 5108 spectra). b) Histogram of the number of nights per target. c) Histogram of the time baselines.

7.1 as (650 au) in 2014. HARPS data from this survey together with the PIONER interferometer data allowed to detect a close low mass stellar companion to HD106906 with a period of 10 days, (Lagrange et al. 2016). The presence of the binary could explain the wide orbit of HD106906b under some circumstances (Rodet et al. 2017).

3.1.3. HD131399

HD131399 is member of a complex hierarchical system. HD131399A forms a binary with the tight binary HD131399BC. A GP companion was discovered with SPHERE around HD131399A by Wagner et al. (2016) but is now identified as a background star with similar proper motion (Nielsen et al. 2017a). We detected in this survey the presence of a close stellar companion to HD131399A, with a period of 10 days (0.1 au), and an $M \sin i$ of $450 M_{\text{Jup}}$ (Lagrange et al. 2017).

3.1.4. HD177171

HD 177171 (ρ Tel) was reported as a spectroscopic binary by Nordström et al. (2004) and as an astrometric binary by Frankowski & Jorissen (2007) from the HIPPARCOS data. This is confirmed by Lagrange et al. (2013) in the feasibility study of this survey. We measure an amplitude of at least 20 km s^{-1} in the RV. Our time sampling does not allow for the estimation the period of this stellar companion.

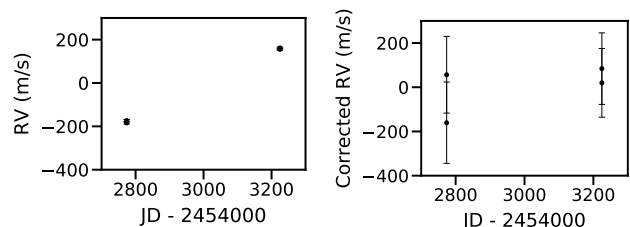


Fig. 3: HD186704 RV long term trend. (*Left*) RV time variations, (*right*) RV corrected from the RV-BVS correlation time variations.

3.1.5. HD186704A

HD186704 is a known binary system with a companion at 10 as (Zuckerman et al. 2013). Nidever et al. (2002) report a trend in the RV of $88 \pm 8 \text{ m s}^{-1} \text{ d}^{-1}$ with a negative curvature based on 4 observations spaced on 70 days for HD186704AB. Tremko et al. (2010) observe a change in the RV of 4200 m s^{-1} in 8682 days on HD186704A. Finally, Tokovinin (2014) reported HD186704A as hosting a spectroscopic binary (SB) companion with a 3990 days period. We observe a trend of 340 m s^{-1} over a duration of 450 days in the RV of HD186704A based on 4 spectra. This corresponds to a slope of $0.75 \text{ m s}^{-1} \text{ d}^{-1}$. The star present signs of activity, we therefore corrected the RV using the RV-BVS correlation using Melo et al. (2007) method (see Appendix B).

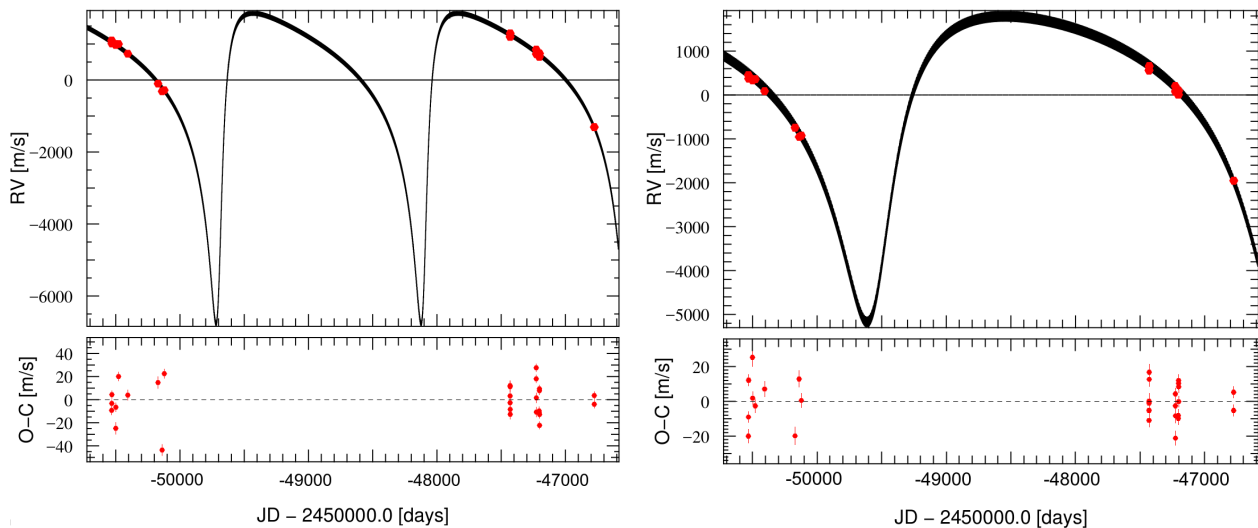


Fig. 4: Solutions of HD181321 RV fit by the sum of two keplerian (*Top*) and their residuals (*Bottom*) . *Left*: 1600 days solution. *Right*: 3200 days solution.

The trend is still visible with a lower slope $0.23 \text{ m s}^{-1} \text{ d}^{-1}$. We present the RV and corrected RV of HD186704A in Figure 3. The difference of one order of magnitude on the slope of the trend between Nidever et al. (2002) observations and ours can be explained by the fact that our observations were made when the SB was closer to the periastron or apastron of its orbit.

3.1.6. HD181321

We confirm that HD181321 is an SB. Nordström et al. (2004) report a variation of 2.3 km s^{-1} over 9 yr, Guenther & Esposito (2007) report a trend with a slope of $1.4 \text{ km s}^{-1} \text{ yr}^{-1}$. Our observations spread on 3757 days (10.3 yr) cover at least two orbital periods. The star is active and show BVS variations with a period of 2 – 2.5 days that should correspond to the rotational period of the star. We use *yorbit* to fit the RV with two Keplerian models, one to fit the stellar activity variation and another to fit the binary variations. We find two possible solutions for the companion, one with a period of 1600 days (2.7 au) and a minimum mass of $0.1 M_{\odot}$, and a second with a period of 3200 days (4.4 au) and a minimum mass of $0.18 M_{\odot}$. In both cases, the eccentricity is ~ 0.5 . We present those two solutions in Figure 4. More data are needed in order to distinguish between those two solutions.

3.1.7. HD206893

HD206893 is a F5V star that hosts a directly imaged BD companion at a separation of 270 mas (Milli et al. 2017; Delorme et al. 2017). We recently reported in Grandjean et al. (2019) a long-term trend in the star RV coupled with pulsations with periods slightly less than one day. We performed an MCMC on both the RV trend, imaging data, and HIPPARCOS-Gaia proper motion measurements to constrain the orbit and dynamical mass of the BD. We concluded that the trend can not be attributed to the BD as it leads to dynamical masses incompatible with the object’s spectra. The presence of an inner companion that

contributes significantly to the RV trend is suggested with a mass of $15 M_{\text{Jup}}$, and a period between 1.6 and 4 yr.

3.1.8. HD217987

HD217987 is a M2V, high proper motion star and exhibits a long-term RV trend induced by its secular acceleration. We therefore corrected the RV from the star secular acceleration in its proper motion we deduced from its parallax and proper motion reported in Gaia Collaboration et al. (2018) (see Figure 5). The corrected RV presents short period variations. The RV and BVS are correlated which indicate that the signal might be dominated by spots or plages (see Figure 5). We observe a long-term variation in $\log R'_{\text{HK}}$, FWHM, and RV which are better fitted by a second degree polynomial model than with a linear model (see Figure 5). This variation could be then attributed to a magnetic cycle of the star with a period greater than 5000 days. An analysis on a large number of M dwarf was made by Mignon et al. (in prep.), including this star and we should expect an offset of $\sim -10 \text{ m s}^{-1}$ in the RV due to the HARPS fiber change of the 15th of June 2015 for this star. We observe an offset in the star’s BVS at this date (see Figure 5), but no significant offset in the RV. We use one template on all the data (see Section 2.3), the impact of the HARPS fiber change is then averaged. This can explain why we do not see a significant RV offset for this star.

3.1.9. HIP36985

HIP36985 is a M2V-type star reported as a wide binary with the system GJ282AB at a separation of $1^{\circ}09$ (Poveda et al. 2009). We observe an RV long-term variation with an amplitude of 700 m s^{-1} on a time baseline of 1400 days in addition to a short-term variation with an amplitude of 50 m s^{-1} . No correlation between RV and BVS is seen, which excludes stellar activity or pulsations as the origin of the long-term variations. The mean $\log R'_{\text{HK}}$ of our spectra of -4.3 indicates that the short-term variations come from magnetic activity (spots). We fit the RV with *yorbit* using two Keplerian models, one to fit the long-term vari-

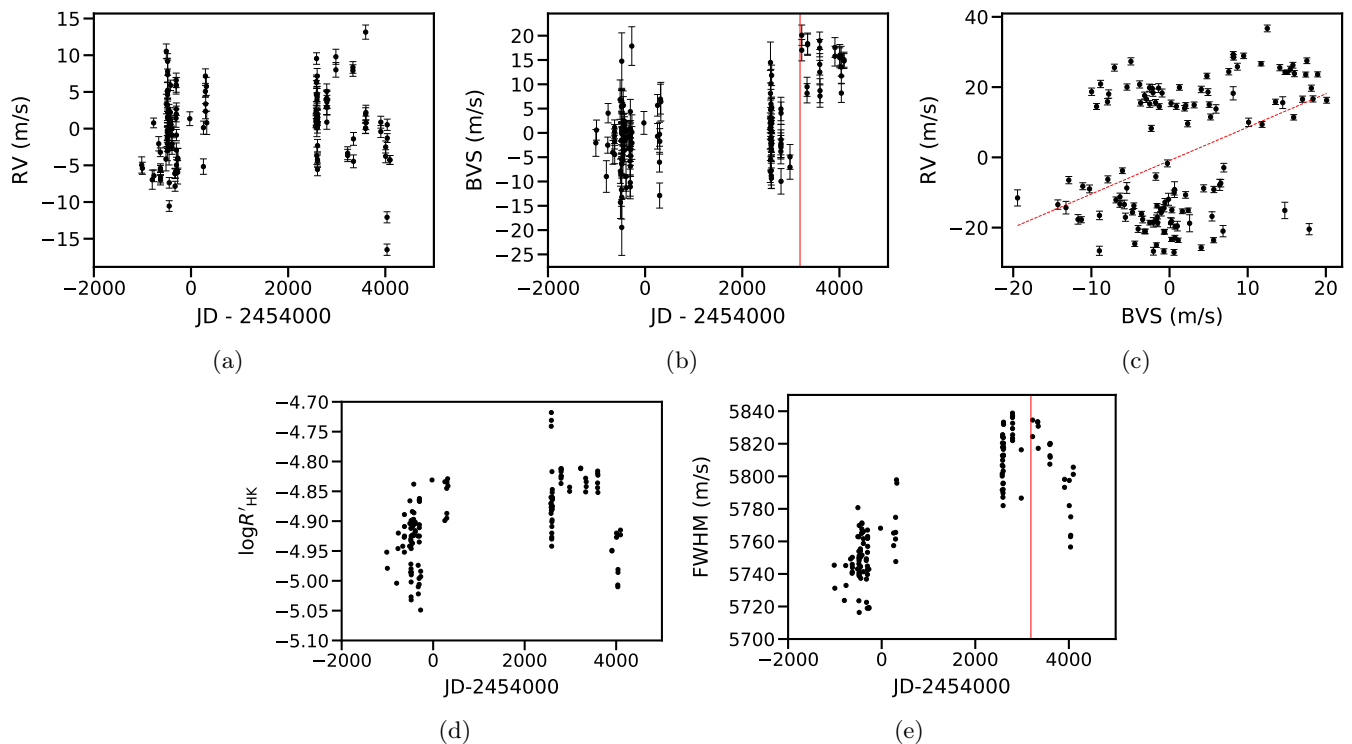


Fig. 5: HD217987 summary. a) RV time variations corrected from the secular acceleration drift. b) BVS time variations, HARPS fiber change is shown with a vertical red line. c) RV corrected from the secular acceleration drift vs BVS. The best linear fit is present in red dashed line. d) $\log R'_{\text{HK}}$ time variations. e) FWHM time variations.

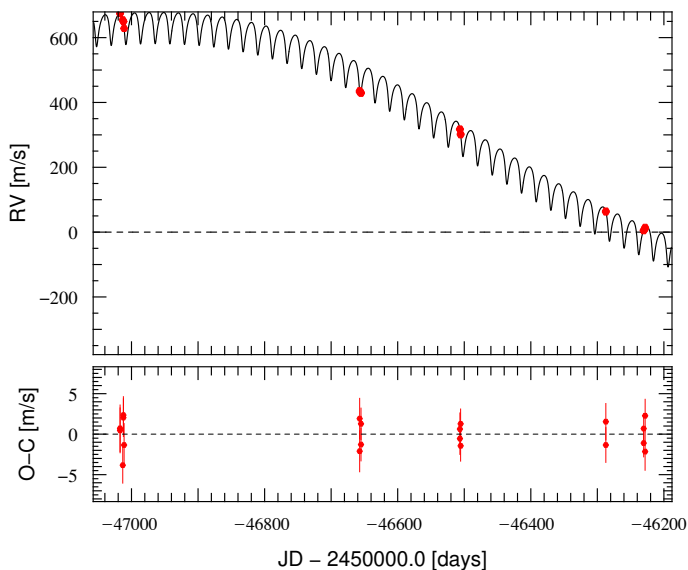


Fig. 6: Solution of HIP36985 RV's fit by a sum of two keplerians and its residuals

ations and an another to fit the companion variations. We present our best solution in Figure 6 and the corresponding companion parameters in Table 1. The companion minimum mass deduced from the present data is $29 M_{\text{Jup}}$ and the period is 8400 days (23 yr), corresponding to a semi-major axis of 7 au and a projected separation of 497 mas. We observed HIP36985 with SPHERE in 2018 and confirm the presence of a however low-mass star companion (Biller et al. in prep.). We find a period of 22 days for the short-

term variations, while the rotation period is of 12 ± 0.1 days (Díez Alonso et al. 2019). The poor sampling of those short-term variations probably explains the strong difference with the rotation period.

Parameters	Value
P (days)	8500^{+1900}_{-1900}
a (au)	$7^{+1}_{-1.1}$
Separation (mas)	500^{+70}_{-80}
e	0.55 ± 0.04
ω ($^{\circ}$)	50 ± 67
K (m s^{-1})	480 ± 230
$M \sin i$ (M_{Jup})	29^{+18}_{-16}

Table 1: HIP36985B's orbital parameters.

3.2. Giant planets

No giant planet companion of period less than 1000 days is detected. In addition to the stars presented in Section 3, some stars presented RV variations without a significant correlation between RV and BVS. For these stars we compared the RV periodogram with the BVS periodogram and the time window periodogram. In all cases, putative periods associated with the RV were also present in the BVS or time window periodograms, or in both. This implies that these RV variations are most likely due to stellar activity or pulsations. We present as an example BD+20 2465 in Figure 7. This star shows RV variations with periods near 2 days which are both present in the time window periodogram and BVS periodogram.

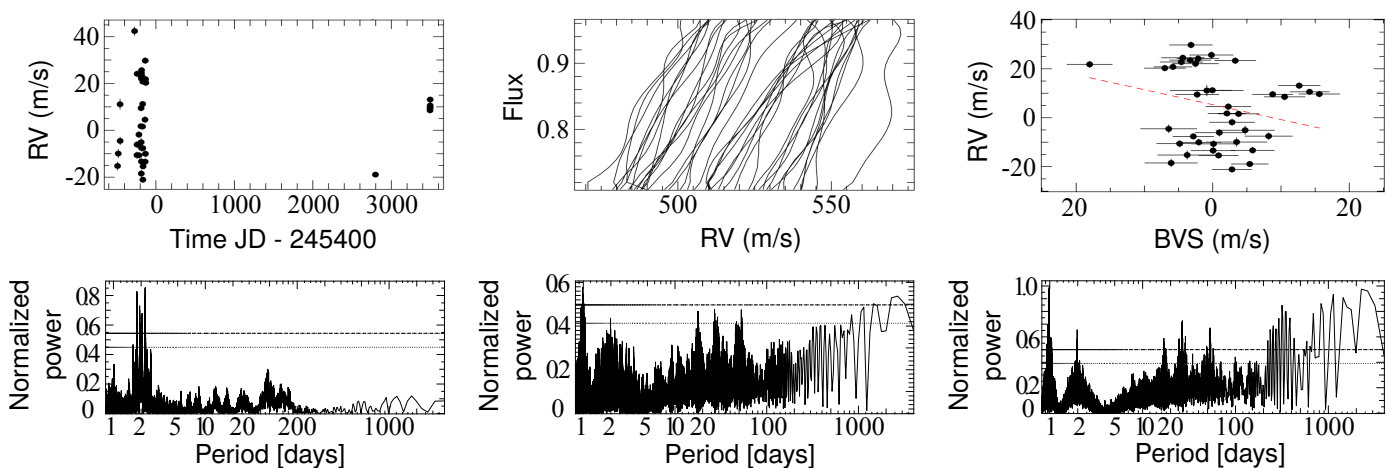


Fig. 7: BD+20 2465 summary. (*Top row*) RV time variations (*Left*), bisectors (*Middle*), RV vs BVS (*Right*). (*Bottom row*) RV periodogram (*Left*), BVS periodogram (*Middle*), time window periodogram (*Right*). The FAP at 1% and 10% are presented respectively in dashed lines and in dotted lines.

4. Analysis

4.1. Stellar intrinsic variability

Figure 8 displays the mean RV uncertainty vs $B - V$, $v \sin i$ and M_* . We also display the RV rms vs $B - V$, and age in Figure 9. We observe that the mean RV uncertainty is correlated to the $v \sin i$ ($Pearson = -0.65$, $p_{value} \ll 1\%$). This is consistent with what is observed on older, AF main sequence stars by Borgniet et al. (2017, 2019). We observe a strong jitter for most of the stars. The ratio between RV rms and the mean RV uncertainty is between 390 and 1 with a median at 16.

The median RV rms is 49 ms^{-1} (300 ms^{-1} on average). This jitter is mainly caused by pulsations for early type stars (from A to F5V), and by spots and faculae for late type stars ($> F5V$). Those two regimes can be distinguished, as stars with pulsations shows a vertical spread of BVS(RV) diagram, whereas stars with spots present a correlation between RV and BVS (Lagrange et al. 2009a). The main origin of RV jitter is reported in Table A.2 for each target.

78 stars out of 89 of our sample present variations in their Ca lines. The median $\log R'_{\text{HK}}$ of our sample is -4.3 with a standard deviation of 0.2. 4 stars present signs of low activity ($\log R'_{\text{HK}} < -4.75$), 59 are active ($-4.75 < \log R'_{\text{HK}} < -4.2$) and 15 stars present signs of high activity ($\log R'_{\text{HK}} > -4.2$). We present in Figure 10 $\log R'_{\text{HK}}$ vs $B - V$. Some early F-type pulsating stars also present signs of activity when all late type stars present signs of activity.

4.2. HARPS fiber change

In June 2015, the fiber of the HARPS instrument was changed in order to increase its stability (Lo Curto et al. 2015). Lo Curto et al. (2015) show that it leads to a change in the instrument profile which impacts the CCF computation and therefore the RV and BVS computation. They observed an offset in the RV between the datasets taken before and after this change of the order of 15 m s^{-1} for old F to K-type stars, based on 19 stars (Lo Curto et al. 2015). A more detailed analysis is currently underway for a

Name	ST	$B - V$	$\langle \text{FWHM} \rangle$ (km s^{-1})	Offset (m s^{-1})	Ratio
HD7661	K0V	0.77	9.2	42	1.4
HD218860	G8V	0.74	11.7	57	1.4

Table 2: Parameters of the stars that present a significant offset. The offset is the difference between the RV mean before and after HARPS' fiber change, and the ratio is the ratio between the offset and the maximum of the rms before and after the fiber change.

large sample of close M-type main sequence stars (Mignon et al. in prep.). In this analysis, two reference spectra are computed, one before the change and one after. Our current set of spectra for each star is not big enough to build reference spectra as done in Mignon et al. (in prep.). The offset is different from one star to the other and its correlation with stellar parameters is not yet determined (spectral type, $v \sin i$ etc.). This offset has not been estimated on young stars before and the impact of high $v \sin i$ and strong jitter is not known. One should be careful before trying to correct this offset in order to not remove signal.

The difference between the mean of the RV before and after the fiber change can be measured, however, it won't probe the offset alone, as long-term variations (star magnetic cycle, unseen companions, etc.) or a bad sampling of the jitter can also induce a difference in the mean of the RV.

We then decided to correct the offset only when it is significant enough. We compared the difference between the RV mean before and after the fiber change to the maximum of the rms before and after the fiber change to determine it. First, we selected the stars for which computing rms before and after the fiber change is relevant : we excluded the stars for which we have less than 10 spectra, less than 6 spectra before the fiber change, and less than 6 spectra after. We excluded the stars identified as SB (marked "B" in Table A.2) or presenting a long-term variation due to a companion (marked "T" in Table A.2). We also excluded the stars for which the RV amplitude is more than 900 m s^{-1} as the offset should be negligible compared to the jitter.

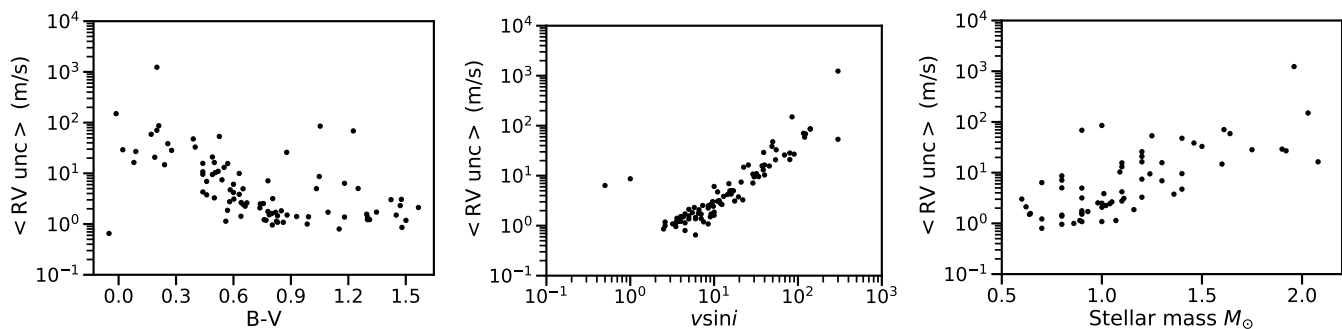


Fig. 8: Summary of the survey RV uncertainties. Mean RV uncertainty (accounting for the photon noise only) vs $B - V$ (Left), vs $v \sin i$ (Middle) and vs M_{\star} (in M_{\odot} , Right).

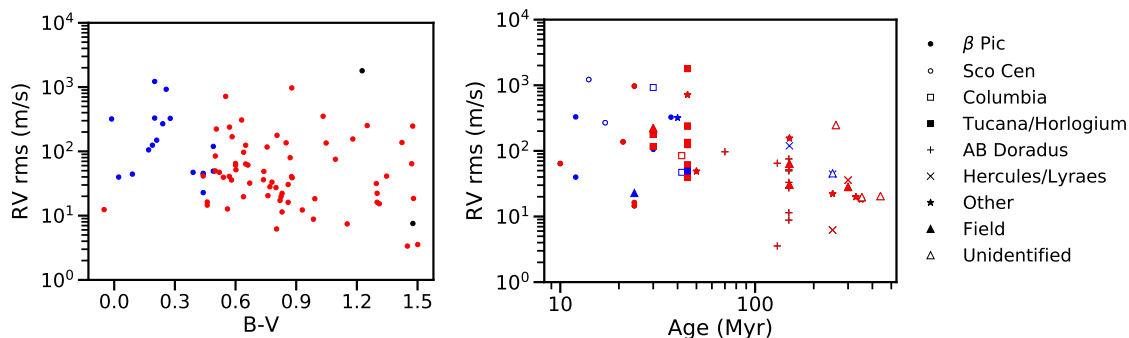


Fig. 9: Survey RV rms summary. (Left) RV rms vs $B - V$, (Right) RV rms and vs age. Pulsating stars are plotted in blue, stars with RV dominated magnetic activity (spots) are plotted in red and stars with undetermined main source of RV are plotted in black. Stars with SB signature are not displayed (HD106906, HD131399, HD177171). HD197890 is not considered due to a too small set of data available.

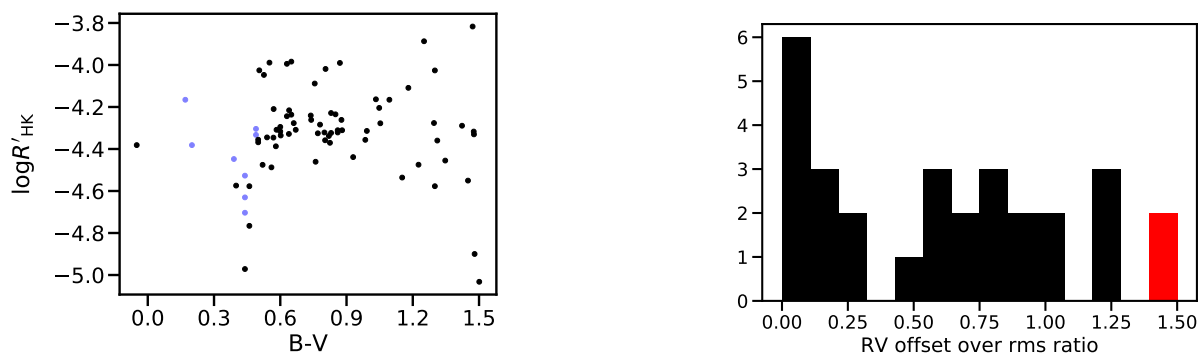


Fig. 10: Survey $\log R'_{HK}$ vs $B - V$. Pulsating stars are plotted in blue.

We finally excluded HD169178 that presents a trend due to a magnetic cycle. Finally, 29 stars were not excluded. We present the histogram of the ratio between the difference in mean of RV between before and after the fiber change and the maximum of the rms before and after the fiber change in Figure 11. We chose to correct the RV offset for the stars that present a ratio larger than 1.3 a threshold that ensure a significant offset. Two stars correspond to this criterion. We present the characteristics of their offset in Table 2, and we present the correction of the offset for one of them in Fig. B.2. They have G to K-types and present an offset of the order of 50 m s^{-1} . Such offsets are three times larger than those found on old stars (Lo Curto et al. 2015).

Fig. 11: Histogram of the ratio between the difference in the RV mean between before and after HARPS' fiber change, and the maximum of the rms before and after the fiber change. The stars that present a ratio greater than 1.3 are plotted in red.

4.3. Exclusion of peculiar stars and RV correction for further analysis

In order to better estimate the number of potentially missed planets in our survey, we excluded some stars from our analyze and made some corrections on others before computing the detection limits. We excluded SB stars (HD106906, HD131399, HD177171, HD181321). Further, we excluded HD116434 since its high value of $v \sin i$ ($> 200 \text{ km s}^{-1}$) prevents the measurements of BVS. We also excluded

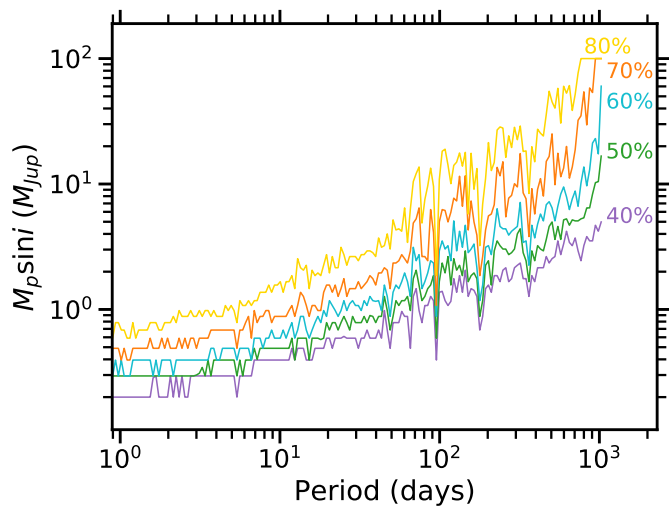


Fig. 12: Search completeness of our survey, corresponding to the lower $m_p \sin i$ for which $X\%$ of the star of the survey have detection limits below this $m_p \sin i$ at a given period P . From bottom to top 40% to 80%.

HD197890 for which our data are too sparse to reliably quantify the detection limits (3 spectra). Thus leads to 83 stars, 23 A-F stars, 52 F-K stars, and 8 K-M stars.

For stars with RV dominated by spots (marked A in the Table A.2) we corrected their RV from the RV-BVS correlation using Melo et al. (2007) method (see Appendix B). We corrected HD217987 RV from its proper motion and HD186704 RV from its long-term trend with a linear regression. For β Pic, we considered the RV corrected from its pulsations as well as β Pic b and c contributions (Lagrange et al. 2019b).

For the stars for which we identified a non ambiguous offset in the RV, we corrected their RV from this offset (see Table 2).

4.4. Detection limits

We compute $m_p \sin i$ detection limits for periods between 1 and 1000 days in the GP domain (between 1 and $13 M_{\text{Jup}}$), and in the BD domain (between 13 and $80 M_{\text{Jup}}$). We use the Local Power Analysis (LPA) (Meunier et al. 2012; Borgniet et al. 2017) which determines, for all periods P , the minimum $m_p \sin i$ for which a companion on a circular orbit with a period P would lead to a signal consistent with the data, by comparing the synthetic companion maximum power of its periodogram to the maximum power of the data periodogram within a small period range around the period P .

We then compute the completeness function $C(m_p \sin i, P)$ which corresponds for a given couple $(m_p \sin i, P)$ to the fraction of stars for which the companion is excluded by the detection limits (Borgniet et al. 2017). We present the 40 to 80% search completeness in Figure 12.

4.5. Companion occurrence rates

We compute the upper limits of companions occurrence rates for our 83 stars in the GP (1 to $13 M_{\text{Jup}}$) and BD

(13 to $80 M_{\text{Jup}}$) domains for AF ($B - V \in [-0.05 : 0.52]$), FK ($B - V \in [0.52 : 1.33]$), KM ($B - V \geq 1.33$) type stars for different ranges of periods : 1-10, 10-100, 100-1000, and 1-1000 days. We use the method described in Borgniet et al. (2017) to compute the occurrence rates and to correct them from the estimated number of missed companions n_{miss} derived from the search completeness.

We present the upper limits of the occurrence rates for all stars in Figure 13 and for AF, FK, M, and all stars in Table 3. The GP occurrence rate is below $2^{+3}_{-2}\%$ (1σ) and the BD occurrence rate is below $1^{+3}_{-1}\%$ (1σ) for periods under 1000 days.

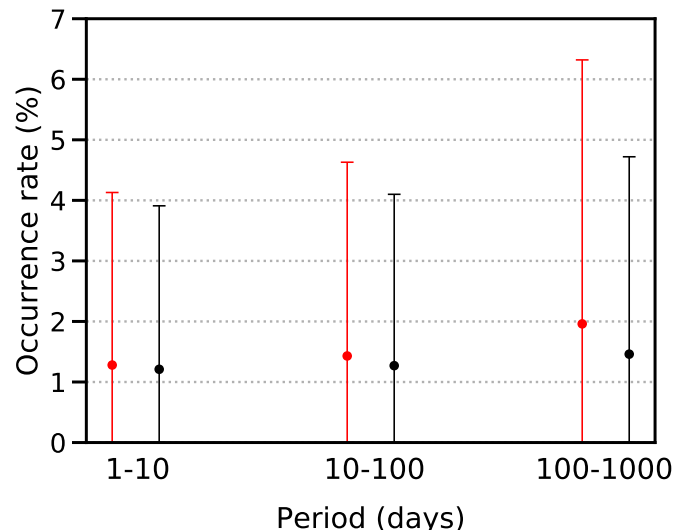


Fig. 13: Upper limits (1σ) on the occurrence rates for our survey for period ranges of 1-10, 10-100, and 100- 1000 days in the GP domain ($1 - 13 M_{\text{Jup}}$, Red) and BD domain ($13 - 80 M_{\text{Jup}}$, Black).

4.6. Comparison to surveys on main sequence stars

No GP companion with periods lower than 1000 days was detected in the present survey. This non-detection is robust for HJ as 70% of the star of the survey have detection limits lower than $1 M_{\text{Jup}}$ for period lower than 10 days. The completeness of the survey is over 71 % for AF and FK stars and $n_{\text{miss}} < 0.4$ for AF and FK stars in the 1- 1000 days domain (*cf* Table 3). However, we may have missed some planets with low masses and long period as only 40% of the stars of the survey have detection limits lower than $5 M_{\text{Jup}}$ between 100 and 1000 days.

We statistically tested if our GP non-detection implies GP occurrence rates around young stars significantly lower than around older main sequence (MS) stars, using the p-value formalism. The p-value is the probability to get the observed results given a null hypothesis, if it is lower than 10% then the null hypothesis can be rejected. We tested the following null hypothesis : GP occurrence rates are identical around young and main sequence stars in the same mass and period range.

We first applied this formalism in the 1- 1000 days domain with a survey that have a completeness similar to ours. For AF MS stars the GP occurrence rate in this domain was estimated at $2.5^{+2.5}_{-0.5}\%$ (Borgniet et al. 2019). We detected

Table 3: GP ($m_p \sin i \in [1, 13] M_{\text{Jup}}$) and BD ($m_p \sin i \in [13, 80] M_{\text{Jup}}$) occurrence rates around young nearby stars. The parameters are displayed in normal, bold, italic or bold and italic fonts when considering the full star sample, the early type AF stars, FK-type stars or KM-type stars, respectively.

$m_p \sin i$ interval (M_{Jup})	Orbital period interval (day)	$B - V$	Search completeness C (%)	Detected GP systems	Missed GP systems upper limit	GP occurrence rate upper limit (%)	Confidence intervals 1σ (%) 2σ (%)	
1-13 (GP)	1-10	all	94	0	0.1	1.3	0 - 4.1	0 - 7.0
		$[-0.05 : 0.52[$	89	0	0.1	4.9	0 - 14.7	0 - 24.0
		$[0.52 : 1.33[$	<i>95</i>	<i>0</i>	<i>0.1</i>	<i>2.0</i>	<i>0 - 6.4</i>	<i>0 - 10.8</i>
		≥ 1.33	98	0	0.0	12.8	0 - 32.9	0 - 50.0
	1-100	all	89	0	0.1	1.4	0 - 4.4	0 - 7.4
		$[-0.05 : 0.52[$	81	0	0.2	5.4	0 - 16.3	0 - 26.7
		$[0.52 : 1.33[$	<i>91</i>	<i>0</i>	<i>0.1</i>	<i>2.1</i>	<i>0 - 6.7</i>	<i>0 - 11.3</i>
		≥ 1.33	92	0.1	0.0	13.6	0 - 35.0	0 - 53.1
	1-1000	all	80	0	0.3	1.5	0 - 4.9	0 - 8.3
$[-0.05 : 0.52[$		71	0	0.4	6.2	0 - 18.6	0 - 30.5	
$[0.52 : 1.33[$		<i>82</i>	<i>0</i>	<i>0.2</i>	<i>2.4</i>	<i>0 - 7.5</i>	<i>0 - 12.6</i>	
	≥ 1.33	86	0	0.2	14.5	0 - 37.4	0 - 56.6	
13-80 (BD)	1-10	all	99	0	0.0	1.2	0 - 3.9	0 - 6.6
		$[-0.05 : 0.52[$	99	0	0.0	4.4	0 - 13.2	0 - 21.6
		$[0.52 : 1.33[$	<i>99</i>	<i>0</i>	<i>0.0</i>	<i>1.9</i>	<i>0 - 6.2</i>	<i>0 - 10.4</i>
		≥ 1.33	99	0	0.0	12.6	0 - 32.6	0 - 49.5
	1-100	all	97	0	0.0	1.2	0 - 4.0	0 - 6.8
		$[-0.05 : 0.52[$	95	0	0.0	4.6	0 - 13.7	0 - 22.5
		$[0.52 : 1.33[$	<i>97</i>	<i>0</i>	<i>0.0</i>	<i>2.0</i>	<i>0 - 6.3</i>	<i>0 - 10.6</i>
		≥ 1.33	93	0	0.1	13.4	0 - 34.7	0 - 52.6
	1-1000	all	92	0	0.1	1.3	0 - 4.2	0 - 7.2
$[-0.05 : 0.52[$		89	0	0.1	4.9	0 - 14.7	0 - 24.0	
$[0.52 : 1.33[$		<i>93</i>	<i>0</i>	<i>0.1</i>	<i>2.1</i>	<i>0 - 6.6</i>	<i>0 - 11.1</i>	
	≥ 1.33	90	0	0.1	13.8	0 - 35.7	0 - 54.1	

0 companion out of 23 stars, the corresponding p-value is 56_{-21}^{+7} %. The null hypothesis can not be rejected.

Then, we applied this formalism in the HJ ($P < 10$ days) domain. For FK MS stars, the occurrence rate for HJ in this domain was estimated at : $0.46_{-0.3}^{+0.3}$ % by Cumming et al. (2008) and at 1.2 ± 0.38 % by Wright et al. (2012). We detected 0 companion out of 52 stars, the corresponding p-value are respectively 79_{-11}^{+13} % and 53_{-9}^{+12} %. The null hypothesis can not be rejected.

There is no evidence for a difference in occurrence rates of HJ between young and MS stars.

BD companions occurrence rates around MS stars is low : $f \leq 1.1_{-1.1}^{+4.1}$ % for periods less than 1000 days (Borgniet et al. 2017), our non detection is not surprising. A bigger sample is needed to determine if BD occurrence rates around young and MS stars are different or not.

5. Conclusions

We observed 89 young A- to M-type stars over 3 years or more with HARPS to search for GP and BD with periods less than 1000 days. This survey allowed to detect close binaries around HD106906 and around HD131399 (Lagrange et al. 2016, 2017). We constrained the period of HD181321B and confirmed the RV trend in HD186704's RV. We also dis-

covered a low-mass star companion to HIP36985. No GP companion was detected in this survey. We obtain upper limits on the GP and BD occurrence rates, they are respectively 2_{-2}^{+3} % and 1_{-1}^{+3} % for periods of less than 1000 days. Our comparison of these occurrence rates to those derived for MS stars (Borgniet et al. 2019; Cumming et al. 2008; Wright et al. 2012) indicates that there is no evidence for a difference in occurrence rates of HJ between young and MS stars.

The forthcoming analysis of our SOPHIE survey around young stars and of our on-going HARPS survey on Sco-Cen stars will add 60 and 80 stars, respectively, in our analysis. This will allow for the derivation of more accurate occurrence rates and it will help in the search for the possible impact of system ages on occurrence rates.

Acknowledgements. We acknowledge support from the French CNRS and from the Agence Nationale de la Recherche (ANR grant GIPSE ANR-14-CE33-0018). This work has been supported by a grant from Labex OSUG@2020 (Investissements d'avenir – ANR10 LABX56). These results have made use of the SIMBAD database, operated at the CDS, Strasbourg, France. ESO SD acknowledges the support by INAF/Frontiera through the "Progetti Premiali" funding scheme of the Italian Ministry of Education, University, and Research

6. References

References

- Ammler-von Eiff, M. & Guenther, E. W. 2009, *A&A*, 508, 677
- Aumann, H. H. 1985, *Publications of the Astronomical Society of the Pacific*, 97, 885
- Backman, D. E. & Gillett, F. C. 1987, in *Lecture Notes in Physics*, Berlin Springer Verlag, Vol. 291, *Cool Stars, Stellar Systems and the Sun*, ed. J. L. Linsky & R. E. Stencel, 340–350
- Bailey, V., Meshkat, T., Reiter, M., et al. 2014, *The Astrophysical Journal Letters*, 780, L4
- Beichman, C. A., Bryden, G., Stapelfeldt, K. R., et al. 2006, *The Astrophysical Journal*, 652, 1674
- Beust, H., Lagrange-Henri, A. M., Vidal-Madjar, A., & Ferlet, R. 1989, *A&A*, 223, 304
- Billar, B., Grandjean, A., & Lagrange, A. M. in prep.
- Bonavita, M., Desidera, S., Thalmann, C., et al. 2016, *A&A*, 593, A38
- Borgniet, S., Lagrange, A. M., Meunier, N., & Galland, F. 2017, *A&A*, 599, A57
- Borgniet, S., Lagrange, A.-M., Meunier, N., et al. 2019, *A&A*, 621, A87
- Bouchy, F. & Sophie Team. 2006, in *Tenth Anniversary of 51 Peg-b: Status of and prospects for hot Jupiter studies*, ed. L. Arnold, F. Bouchy, & C. Moutou, 319–325
- Brandt, T. D., Kuzuhara, M., McElwain, M. W., et al. 2014, *The Astrophysical Journal*, 786, 1
- Carpenter, J. M., Bouwman, J., Mamajek, E. E., et al. 2009, *The Astrophysical Journal Supplement Series*, 181, 197
- Chauvin, G., Desidera, S., Lagrange, A.-M., et al. 2017a, in *SF2A-2017: Proceedings of the Annual meeting of the French Society of Astronomy and Astrophysics*, ed. C. Reylé, P. Di Matteo, F. Herpin, E. Lagadec, A. Lançon, Z. Meliani, & F. Royer, 331–335
- Chauvin, G., Desidera, S., Lagrange, A.-M., et al. 2017b, *A&A*, 605, L9
- Chen, C. H., Mittal, T., Kuchner, M., et al. 2014, *The Astrophysical Journal Supplement Series*, 211, 25
- Chen, C. H., Patten, B. M., Werner, M. W., et al. 2005, *The Astrophysical Journal*, 634, 1372
- Choquet, E., Perrin, M. D., Chen, C. H., et al. 2016, *The Astrophysical Journal Letters*, 817, L2
- Churcher, L., Wyatt, M., & Smith, R. 2011, *Monthly Notices of the Royal Astronomical Society*, 410, 2
- Cumming, A., Butler, R. P., Marcy, G. W., et al. 2008, *PASP*, 120, 531
- de la Reza, R. & Pinzón, G. 2004, *The Astronomical Journal*, 128, 1812
- Delorme, P., Lagrange, A. M., Chauvin, G., et al. 2012, *A&A*, 539, A72
- Delorme, P., Schmidt, T., Bonnefoy, M., et al. 2017, *A&A*, 608, A79
- Desidera, S., Covino, E., Messina, S., et al. 2015, *A&A*, 573, A126
- Desort, M., Lagrange, A. M., Galland, F., Udry, S., & Mayor, M. 2007, *A&A*, 473, 983
- Díez Alonso, E., Caballero, J. A., Montes, D., et al. 2019, *A&A*, 621, A126
- Donaldson, J. K., Roberge, A., Chen, C. H., et al. 2012, *The Astrophysical Journal*, 753, 147
- Donati, J. F., Moutou, C., Malo, L., et al. 2016, *Nature*, 534, 662
- Esoposito, M., Guenther, E., Hatzes, A. P., & Hartmann, M. 2006, in *Tenth Anniversary of 51 Peg-b: Status of and prospects for hot Jupiter studies*, ed. L. Arnold, F. Bouchy, & C. Moutou, 127–134
- Figueira, P., Marmier, M., Bonfils, X., et al. 2010, *A&A*, 513, L8
- Folsom, C. P., Bouvier, J., Petit, P., et al. 2018, *MNRAS*, 474, 4956
- Frankowski, A. & Jorissen, A. 2007, *Baltic Astronomy*, 16, 104
- Fuhrmann, K., Chini, R., Kaderhandt, L., & Chen, Z. 2017, *ApJ*, 836, 139
- Gaia Collaboration, Brown, A. G. A., Vallenari, A., et al. 2018, *A&A*, 616, A1
- Galland, F., Lagrange, A. M., Udry, S., et al. 2005a, *A&A*, 444, L21
- Galland, F., Lagrange, A. M., Udry, S., et al. 2005b, *A&A*, 443, 337
- Gallet, F. & Bouvier, J. 2015, *A&A*, 577, A98
- Golimowski, D. A., Krist, J. E., Stapelfeldt, K. R., et al. 2011, *The Astronomical Journal*, 142, 30
- Grandjean, A., Lagrange, A. M., Beust, H., et al. 2019, *A&A*, 627, L9
- Guenther, E. W. & Esoposito, E. 2007, *ArXiv Astrophysics e-prints* [[astro-ph/0701293](https://arxiv.org/abs/astro-ph/0701293)]
- Hillenbrand, L. A., Carpenter, J. M., Kim, J. S., et al. 2008, *The Astrophysical Journal*, 677, 630
- Hobbs, L. M., Vidal-Madjar, A., Ferlet, R., Albert, C. E., & Gry, C. 1985, *ApJ*, 293, L29
- Holland, W. S., Greaves, J. S., Zuckerman, B., et al. 1998, *Nature*, 392, 788
- Huélamo, N., Figueira, P., Bonfils, X., et al. 2008, *A&A*, 489, L9
- Kalas, P., Liu, M. C., & Matthews, B. C. 2004, *Science*, 303, 1990
- Kiefer, F., Lecavelier des Etangs, A., Boissier, J., et al. 2014, *Nature*, 514, 462
- Kiraga, M. 2012, *Acta Astron.*, 62, 67
- Kley, W. & Nelson, R. P. 2012, *ARA&A*, 50, 211
- Koen, C. & Eyer, L. 2002, *MNRAS*, 331, 45
- Kovári, Z., Strassmeier, K., Granzer, T., et al. 2004, *Astronomy and Astrophysics*, 417, 1047
- Lagrange, A. M., Boccaletti, A., Langlois, M., et al. 2019a, *A&A*, 621, L8
- Lagrange, A. M., De Bondt, K., Meunier, N., et al. 2012, *A&A*, 542, A18
- Lagrange, A. M., Desort, M., Galland, F., Udry, S., & Mayor, M. 2009a, *A&A*, 495, 335
- Lagrange, A. M., Gratadour, D., Chauvin, G., et al. 2009b, *A&A*, 493, L21
- Lagrange, A.-M., Keppler, M., Beust, H., et al. 2017, *A&A*, 608, L9
- Lagrange, A.-M., Mathias, P., & Absil, O. 2016, *A&A*, submitted
- Lagrange, A.-M., Meunier, N., Chauvin, G., et al. 2013, *A&A*, 559, A83
- Lagrange, A. M., Meunier, N., Rubini, P., et al. 2019b, *Nature Astronomy*, 421
- Lagrange-Henri, A. M., Vidal-Madjar, A., & Ferlet, R. 1988, *A&A*, 190, 275
- Lawler, S. M., Beichman, C. A., Bryden, G., et al. 2009, *The Astrophysical Journal*, 705, 89
- Lindgren, S. & Heiter, U. 2017, *A&A*, 604, A97
- Lo Curto, G., Pepe, F., Avila, G., et al. 2015, *The Messenger*, 162, 9
- Mamajek, E. E. 2012, *The Astrophysical Journal Letters*, 754, L20
- Mamajek, E. E., Meyer, M. R., Hinz, P. M., et al. 2004, *ApJ*, 612, 496
- Mannings, V. & Barlow, M. J. 1998, *The Astrophysical Journal*, 497, 330
- Mayor, M., Pepe, F., Queloz, D., et al. 2003, *The Messenger*, 114, 2
- McDonald, I., Zijlstra, A. A., & Boyer, M. L. 2012, *Monthly Notices of the Royal Astronomical Society*, 427, 343
- Melo, C., Santos, N. C., Gieren, W., et al. 2007, *A&A*, 467, 721
- Meshkat, T., Bailey, V., Rameau, J., et al. 2013, *The Astrophysical Journal*, 775, L40
- Messina, S., Desidera, S., Turatto, M., Lanzafame, A. C., & Guinan, E. F. 2010, *A&A*, 520, A15
- Messina, S., Millward, M., Buccino, A., et al. 2017, *A&A*, 600, A83
- Meunier, N., Lagrange, A. M., & De Bondt, K. 2012, *A&A*, 545, A87
- Meyer, M. R., Carpenter, J. M., Mamajek, E. E., et al. 2008, *The Astrophysical Journal Letters*, 673, L181
- Meyer, M. R., Hillenbrand, L. A., Backman, D., et al. 2006, *Publications of the Astronomical Society of the Pacific*, 118, 1690
- Meyer, M. R., Hillenbrand, L. A., Backman, D. E., et al. 2004, *The Astrophysical Journal Supplement Series*, 154, 422
- Mignoul, L., Bonfils, X., & Delfosse, X. in prep.
- Milli, J., Hibon, P., Christiaens, V., et al. 2017, *A&A*, 597, L2
- Montesinos, B., Eiroa, C., Mora, A., & Merín, B. 2009, *A&A*, 495, 901
- Montet, B. T., Crepp, J. R., Johnson, J. A., Howard, A. W., & Marcy, G. W. 2014, *The Astrophysical Journal*, 781, 28
- Morales, F. Y., Bryden, G., Werner, M. W., & Stapelfeldt, K. R. 2016, *The Astrophysical Journal*, 831, 97
- Morin, J., Donati, J. F., Petit, P., et al. 2008, *MNRAS*, 390, 567
- Moro-Martín, A., Marshall, J. P., Kennedy, G., et al. 2015, *ApJ*, 801, 143
- Moór, A., Ábrahám, P., Kóspál, A., et al. 2013, *The Astrophysical Journal Letters*, 775, L51
- Nidever, D. L., Marcy, G. W., Butler, R. P., Fischer, D. A., & Vogt, S. S. 2002, *The Astrophysical Journal Supplement Series*, 141, 503
- Nielsen, E. L., De Rosa, R. J., Rameau, J., et al. 2017a, *AJ*, 154, 218
- Nielsen, E. L., De Rosa, R. J., Rameau, J., et al. 2017b, *AJ*, 154, 218
- Nordström, B., Mayor, M., Andersen, J., et al. 2004, *A&A*, 418, 989
- Olmedo, M., Chávez, M., Bertone, E., & De la Luz, V. 2013, *PASP*, 125, 1436
- Passegger, V. M., Reiners, A., Jeffers, S. V., et al. 2018, *A&A*, 615, A6
- Patel, R. I., Metchev, S. A., & Heinze, A. 2014, *The Astrophysical Journal Supplement Series*, 212, 10
- Paulson, D. B. & Yelda, S. 2006, *PASP*, 118, 706
- Pecaut, M. J., Mamajek, E. E., & Bubar, E. J. 2012, *The Astrophysical Journal*, 746, 154

- Plavchan, P., Werner, M. W., Chen, C. H., et al. 2009, *The Astrophysical Journal*, 698, 1068
- Pollack, J. B., Hubickyj, O., Bodenheimer, P., et al. 1996, *Icarus*, 124, 62
- Poveda, A., Allen, C., Costero, R., Echevarría, J., & Hernández-Alcántara, A. 2009, *The Astrophysical Journal*, 706, 343
- Rameau, J., Chauvin, G., Lagrange, A.-M., et al. 2013, *The Astrophysical Journal Letters*, 772, L15
- Rameau, J., Chauvin, G., Lagrange, A. M., et al. 2013, *A&A*, 553, A60
- Rebull, L. M., Stapelfeldt, K. R., Werner, M. W., et al. 2008, *The Astrophysical Journal*, 681, 1484
- Rebull, L. M., Stauffer, J. R., Bouvier, J., et al. 2016, *The Astronomical Journal*, 152, 114
- Rhee, J. H., Song, I., Zuckerman, B., & McElwain, M. 2007, *ApJ*, 660, 1556
- Rodet, L., Beust, H., Bonnefoy, M., et al. 2017, *A&A*, 602, A12
- Schneider, G., Silverstone, M. D., Hines, D. C., et al. 2006, *The Astrophysical Journal*, 650, 414
- Ségransan, D., Mayor, M., Udry, S., et al. 2011, *A&A*, 535, A54
- Sierchio, J. M., Rieke, G. H., Su, K. Y. L., & Gáspár, A. 2014, *The Astrophysical Journal*, 785, 33
- Simon, M. & Schaefer, G. H. 2011, *The Astrophysical Journal*, 743, 158
- Smith, B. A. & Terrile, R. J. 1984, *Science*, 226, 1421
- Soto, M. G., Jenkins, J. S., & Jones, M. I. 2015, *Monthly Notices of the Royal Astronomical Society*, 451, 3131
- Sommer, R., Perrin, M. D., Pueyo, L., et al. 2014, *The Astrophysical Journal Letters*, 786, L23
- Stauffer, J., Rebull, L., Bouvier, J., et al. 2016, *The Astronomical Journal*, 152, 115
- Strassmeier, K. G., Pichler, T., Weber, M., & Granzer, T. 2003, *A&A*, 411, 595
- Teyssandier, J., Lai, D., & Vick, M. 2019, *MNRAS*, 486, 2265
- Tokovinin, A. 2014, *The Astronomical Journal*, 147, 87
- Tremko, J., Bakos, G. A., Žižňovský, J., & Pribulla, T. 2010, *Contributions of the Astronomical Observatory Skalnaté Pleso*, 40, 83
- van Leeuwen, F. 2007, *A&A*, 474, 653
- Vigan, A., Bonavita, M., Biller, B., et al. 2017, *A&A*, 603, A3
- Wagner, K., Apai, D., Kasper, M., et al. 2016, *Science*, 353, 673
- Weise, P., Launhardt, R., Setiawan, J., & Henning, T. 2010, *A&A*, 517, A88
- Wright, J. T., Marcy, G. W., Howard, A. W., et al. 2012, *The Astrophysical Journal*, 753, 160
- Wright, N. J., Drake, J. J., Mamajek, E. E., & Henry, G. W. 2011, *ApJ*, 743, 48
- Yu, L., Donati, J.-F., Hébrard, E. M., et al. 2017, *MNRAS*, 467, 1342
- Zuckerman, B., Rhee, J. H., Song, I., & Bessell, M. S. 2011, *The Astrophysical Journal*, 732, 61
- Zuckerman, B. & Song, I. 2004, *The Astrophysical Journal*, 603, 738
- Zuckerman, B., Vican, L., Song, I., & Schneider, A. 2013, *The Astrophysical Journal*, 778, 5
- Zuckerman, B., Vican, L., Song, I., & Schneider, A. 2013, *ApJ*, 778, 5

Appendix A: Sample

Table A.1: Stars characteristics for the 89 stars of our HARPS RV survey. Spectral type (ST) and $B - V$ values are taken from the CDS database. The $v \sin i$ values are taken from the CDS if present, or are computed with SAFIR based on the CCF width. The IR/D column report if either an IR excess is reported (y) or not (n) and if a disc has been imaged (y) or not (n) in the literature.

Name HD/BD/CD	HIP	ST	$B - V$	Mass (M_{\odot})	Age (Myr)	$v \sin i$ (km.s^{-1})	Rotation period (days)	IR/D
HD105	490	G0V	0.600	1.1 ^b	45 ₁₀ ^{5b}	14.5	-	y^c/y^c
HD984	1134	F7V	0.500	1.2 ^b	42 ₇ ^{8b}	40.0	-	-/ n^d
HD987	1113	G8V	0.756	0.98 ^e	30 ₁₅ ^{15d}	7.3	3.72 ± 0.01 ^f	n^g/y^e
HD1466	1481	F8V	0.540	1.2 ^b	45 ₁₀ ^{5b}	21.0	-	y^h/y^i
HD3221	2729	K4V	1.226	0.9 ^f	45 ₁₀ ^{5b}	123.0	0.370 ± 0.002 ^f	n^j/y^i
HD6569	5191	K1V	0.830	0.8 ^b	149 ₄₉ ^{31b}	6.0	7.13 ± 0.05 ^f	-/-
HD7661	5938	K0V	0.770	-	300 ₅₀ ^{50d}	7.5	7.46 ^k	n^l/n^i
HD10008	7576	K0V	0.803	0.8 ^b	250 ₅₀ ^{50b}	3.5	7.15 ± 0.10 ^m	y^n/y^o
HD16765	12530	F71V	0.520	-	-	32.0	-	-/-
HD17925	13402	K1V	0.860	0.9 ^b	150 ₈₀ ^{150b}	8.5	6.76 ^k	$y^p/-$
HD18599	13754	K2V	0.880	-	-	4.3	-	-/-
HD19668	14684	K0V	0.780	0.9 ^b	149 ₄₉ ^{31b}	6.5	5.46 ± 0.08 ^f	y^q/y^d
HD24916	18512	K4V	1.152	0.7 ^r	-	4.5	-	-/-
HD25457	18859	F6V	0.500	1.2 ^b	149 ₄₉ ^{31b}	22.0	3.13 ^k	$y^s/-$
HD26923	19859	G0IV	0.560	1.07 ^r	-	3.5	-	-/-
HD29391	21547	F0IV	0.277	1.75 ^t	37 ₉ ^{9am}	80.0	-	$y^o/-$
HD30447	22226	F3V	0.390	1.4 ^b	42 ₇ ^{8b}	50.0	-	y^u/y^v
HD35650	25283	K6V	1.311	0.7 ^f	-	4.0	9.34 ± 0.08 ^f	y^s/y^w
HD37572	26373	K0V	1.094	0.9 ^e	149 ₄₉ ^{31b}	9.2	4.52 ± 0.02 ^f	y^s/n^e
HD39060	27321	A6V	0.170	1.64 ^e	30 ^e	130.0	-	y^x/y^y
HD41593	28954	K0V	0.825	1.01 ^r	329 ₉₃ ⁹³ⁿ	4.5	-	-/-
HD43989	30030	G0V	0.570	1.1 ^b	45 ₁₀ ^{5b}	45.5	1.15 ^k	y^q/y^d
HD44627	30034	K1V	0.805	0.9 ^f	30 ₁₅ ^{15d}	11.5	3.85 ± 0.01 ^f	-/ n^d
HD45081	29964	K4V	1.251	0.8 ^f	-	16.4	2.67 ± 0.01 ^f	n^z/y^d
HD45270	30314	G1V	0.602	1.11 ^e	149 ₄₉ ^{31b}	17.6	-	y^q/n^e
HD59967	36515	G3V	0.639	1.09 ⁿ	353 ₅₈ ⁵⁸ⁿ	4.0	-	$y^n/-$
HD61005	36948	G8V	0.740	1.0 ^b	50 ₁₀ ^{20b}	8.5	5.04 ± 0.03 ^{aa}	y^{ab}/y^{ac}
HD63608	37923	K0V	0.830	1.0 ^b	250 ₅₀ ^{50b}	3.2	-	-/-
HD77825	44526	K2V	0.992	0.8 ^b	350 ₁₅₀ ^{150b}	7.0	8.64 ^{ad}	-/-
HD82558	46816	K1V	0.870	0.8 ^{ae}	-	29.0	1.70 ^k	-/-
HD89449	50564	F6IV	0.440	-	-	16.0	-	-/-
HD90905	51386	F5V	0.569	1.16 ^e	170 ₇₀ ^{180b}	10.0	2.60 ^k	y^q/y^{af}
HD92945	52462	K1V	0.877	0.9 ^b	170 ₇₀ ^{130b}	4.0	-	n^{ag}/y^{ah}
HD95086	53524	A8III	0.240	1.6 ^{ai}	17 ₄ ^{4aj}	22.5	-	y^{ak}/y^{al}

^b Vigan et al. (2017) ^c Meyer et al. (2004) ^d Weise et al. (2010) ^e Lagrange et al. (2013) ^f Messina et al. (2010) ^g Rebull et al. (2008) ^h Sierchio et al. (2014) ⁱ Mamajek et al. (2004) ^j Donaldson et al. (2012) ^k Wright et al. (2011) ^l Lawler et al. (2009) ^m Folsom et al. (2018) ⁿ Plavchan et al. (2009) ^o Patel et al. (2014) ^p Hillenbrand et al. (2008) ^q Carpenter et al. (2009) ^r Ammler-von Eiff & Guenther (2009) ^s Zuckerman et al. (2011) ^t Simon & Schaefer (2011) ^u Chen et al. (2014) ^v Soummer et al. (2014) ^w Choquet et al. (2016) ^x Aumann (1985) ^y Smith & Terrile (1984) ^z McDonald et al. (2012) ^{aa} Folsom et al. (2018) ^{ab} Meyer et al. (2008) ^{ac} Meyer et al. (2006) ^{ad} Kiraga (2012) ^{ae} Kovári et al. (2004) ^{af} Morales et al. (2016) ^{ag} Chen et al. (2005) ^{ah} Golimowski et al. (2011) ^{ai} Rameau et al. (2013) ^{aj} Meshkat et al. (2013) ^{ak} Rhee et al. (2007) ^{al} Moór et al. (2013)

Table A.1: Continued.

Name HD/BD/CD	HIP	ST	$B - V$	Mass (M_{\odot})	Age (Myr)	$v \sin i$ (km.s^{-1})	Rotation period (days)	IR/D
HD95650	53985	M2V	1.477	0.59 ^{am}	-	11.0	14.80 ^{an}	-/-
HD99211	55705	A7V	0.210	-	-	140.0	-	y ^{ao} /-
HD102458	57524	G4V	0.630	1.70 ^{ap}	-	31.0	-	y ^g /n ^e
HD103743	58241	G4V	0.670	-	-	9.0	-	-/-
HD105690	59315	G5V	0.661	1.02 ^e	8 ₈ ^{15d}	8.5	-	-/-
HD106906	59960	F5V	0.400	1.5 ^{aq}	13 ₂ ^{2ar}	55.0	-	y ^{as} /y ^{at}
HD108767	60965	K0V	-0.050	2.74 ^{au}	-	6.0	-	-/-
HD116434	65426	A2V	0.200	1.96 ^{av}	14 ₄ ^{4av}	300.0	-	n ^{av} /-
HD118100	66252	K5V	1.180	0.7 ^b	150 ₅₀ ^{50b}	0.5	3.96 ^k	-/-
HD131399	72940	A1V	0.080	2.08 ^{aw}	21 ₃ ^{4aw}	25.6	-	-/-
HD141943	-	G2V	0.505	1.09 ^e	30 ₁₅ ^{15d}	40.0	2.2 ^{an}	-/n ^e
HD146464	79958	K3V	1.033	-	-	17.0	2.329 ^{ax}	-/-
HD146624	79881	A0V	0.022	1.9 ^e	12 ^e	39.0	-	-/n ^e
HD152555	82688	F8V	0.600	-	130 ₂₀ ^{20ay}	10.0	2.77 ^k	n ^s /n ^d
HD159492	86305	A5IV	0.189	-	-	54.0	-	-/y ^{az}
HD164249	88399	F6V	0.460	1.3 ^b	24 ₅ ^{5b}	15.0	-	y ^u /-
HD169178	-	K0V	0.850	-	-	5.5	-	-/-
HD171488	91043	G2V	0.551	1.1 ^b	45 ₂₅ ^{35b}	38.5	1.3371 ± 0.0002 ^{ba}	-/-
HD172555	92024	A7V	0.200	1.61 ^e	12 ^{bb}	116.5	-	y ^e /y ^e
HD174429	92680	G9IV	0.878	1.2 ^b	24 ₅ ^{5b}	69.0	0.944 ± 0.001 ^{bb}	y ^u /-
HD177171	93815	F6V	0.526	1.25 ^{ap}	30 ^e	300.0	4.737 ^{ax}	-/n ^e
HD181321	95149	G2V	0.630	0.89 ^{bc}	-	13.0	5.7 ^{bd}	-/-
HD181327	95270	F6V	0.460	1.36 ^e	24 ₅ ^{5b}	19.5	-	y ^{ao} /y ^{be}
HD183414	96334	G3V	0.650	1.04 ^e	150 ₈₀ ^{70b}	9.8	3.924 ^{ax}	-/-
HD186704	97255	G0V	0.583	1.4 ^{bf}	100 ^{bg}	11.0	3.511 ^{an}	y ^z /-
HD188228	98495	A0V	-0.013	2.03 ^e	40 ^e	85.0	-	-/n ^e
HD189245	98470	F7V	0.490	1.2 ^b	150 ₅₀ ^{150b}	80.0	1.88 ± 0.01 ^{bh}	-/-
HD191089	99273	F5V	0.440	1.3 ^b	24 ₅ ^{5d}	37.3	0.488 ± 0.005 ^{bh}	y ^{ao} /y ^{bi}
HD197481	102409	M1V	1.423	0.6 ^f	21 ₅ ^{7ay}	9.6	4.84 ± 0.02 ^f	y ^{bj} /y ^{bk}
HD197890	102626	K3V	1.053	1.0 ^b	45 ₃₅ ^{55b}	140.0	0.3804 ^{an}	y ^z /-
HD202917	105388	G7V	0.650	0.9 ^b	45 ₁₀ ^{5b}	15.4	3.36 ± 0.01 ^f	y ^o /y ^v
HD206860	107350	G0V	0.580	1.1 ^b	300 ₁₀₀ ^{700b}	12.0	4.86 ^k	y ^u /y ^{bl}
HD206893	107412	F5V	0.440	1.24 ^{bm}	250 ₂₀₀ ^{450bn}	29.0	-	y ^{as} /y ^{bm}
HD207575	107947	F6V	0.490	1.24 ^e	45 ₁₅ ^{5b}	30.0	-	y ^s /n ^e
HD213845	111449	F7V	0.440	1.4 ^b	250 ₅₀ ^{750b}	34.0	-	y ^{bo} /-
HD215641	112491	G8V	0.760	-	440 ₄₀ ^{40ay}	3.6	-	-/-
HD216956	113368	A3V	0.090	1.92 ^{bp}	440 ₄₀ ^{40bp}	90.0	-	y ^{bq} /y ^{br}

^{am} Montet et al. (2014) ^{an} Kiraga (2012) ^{ao} Mannings & Barlow (1998) ^{ap} de la Reza & Pinzón (2004) ^{aq} Bailey et al. (2014) ^{ar} Pecaut et al. (2012) ^{as} Sierchio et al. (2014) ^{at} Kalas et al. (2004) ^{au} Montesinos et al. (2009) ^{av} Chauvin et al. (2017b) ^{aw} Nielsen et al. (2017b) ^{ax} Koen & Eyer (2002) ^{ay} Brandt et al. (2014) ^{az} Morales et al. (2016) ^{ba} Strassmeier et al. (2003) ^{bb} Messina et al. (2017) ^{bc} Fuhrmann et al. (2017) ^{bd} Olmedo et al. (2013) ^{be} Schneider et al. (2006) ^{bf} Bonavita et al. (2016) ^{bg} Zuckerman et al. (2013) ^{bh} Desidera et al. (2015) ^{bi} Churcher et al. (2011) ^{bj} Rameau et al. (2013) ^{bk} Kalas et al. (2004) ^{bl} Moro-Martín et al. (2015) ^{bm} Milli et al. (2017) ^{bn} Delorme et al. (2017) ^{bo} Beichman et al. (2006) ^{bp} Mamajek (2012) ^{bq} Backman & Gillett (1987) ^{br} Holland et al. (1998)

Table A.1: Continued.

Name HD/BD/CD	HIP	ST	$B - V$	Mass (M_{\odot})	Age (Myr)	$v \sin i$ (km.s^{-1})	Rotation period (days)	IR/D
HD217343	113579	G5V	0.640	1.05^b	70^e	12.4	-	$-/n^e$
HD217987	114046	M2V	1.480	0.47^{am}	$100 - 10000^{bs}$	2.5	-	$-/-$
HD218396	114189	A5V	0.257	1.46^b	30^e	49.0	-	y^{bt}/y^{ak}
HD218860	114530	G8V	0.738	1.0^f	-	6.6	5.17 ± 0.02^f	$y^s/-$
HD221575	116258	K2V	0.930	-	-	3.6	-	$-/-$
HD223340	-	K1V	0.820	-	-	7.0	-	$-/-$
HD224228	118008	K2V	0.985	0.86^e	149_{49}^{31b}	2.6	-	y^s/n^e
-	6276	G9V	0.800	0.9^b	149_{49}^{31b}	10.0	6.40^k	y^{as}/y^d
-	116384	K7V	1.347	-	-	4.5	-	$-/-$
-	17157	K7V	1.300	-	-	5.0	-	$-/-$
-	23309	M0V	1.471	0.55^{ap}	10_3^d	5.8	8.60 ± 0.07^f	$-/n^g$
-	31878	K7V	1.296	0.643^{bu}	-	5.0	9.06 ± 0.08^f	$-/-$
-	36985	M2V	1.476	0.621^{bv}	260_{260}^{420bw}	5.0	12.16^{an}	$-/-$
-	44722	K7V	1.450	0.638^{bu}	-	9.0	-	$-/-$
-	46634	G5V	0.860	-	-	6.0	3.05 ± 0.03^f	$-/-$
-	51317	M2V	1.501	-	130_{20}^{40ay}	2.6	-	$-/-$
BD+20 2465	-	M5V	1.300	0.42^{bx}	-	3.8	2.60^k	$-/-$
CD-46 1064	-	K3V	1.048	0.8^b	45_{10}^5b	1.0	3.74 ± 0.04^f	$-/-$

^{bs} Delorme et al. (2012) ^{bt} Zuckerman & Song (2004) ^{bu} Lindgren & Heiter (2017) ^{bv} Passegger et al. (2018) ^{bw} Poveda et al. (2009) ^{bx} Morin et al. (2008)

Table A.2: Results for the 89 stars of our HARPS RV survey. Spectral type (ST) are taken from the CDS database. The survey results include the time baseline (TBL), the number of computed spectra N_m , the amplitude corresponding to the difference between the maximum and the minimum of the RV (A), rms and mean uncertainty $\langle U \rangle$ on the RV and BVS measurements, the RV-BVS correlation factor (slope of the best linear fit), the mean FWHM ($\langle \text{FWHM} \rangle$), and the mean $\log R'_{\text{HK}}$ ($\langle \log R'_{\text{HK}} \rangle$). V stands for the dominant source of RV variations, with A for stellar activity (spots), P for pulsations, B for binary and, T for long-term trend.

Stellar characteristics		Survey results.										
Name	HIP	ST	TBL	N_m	RV		BVS		RV-	$\langle \text{FWHM} \rangle$	$\langle \log R'_{\text{HK}} \rangle$	V
HD/BD/CD		(day)			A	rms	$\langle U \rangle$	A	rms	corr.		
					(ms ⁻¹)			(ms ⁻¹)			(km s ⁻¹)	
HD105	490	G0V	4606	36	236.8	61.1	4.2	310.7	9.8	72.9	-0.67	A
HD984	1134	F7V	867	21	301.9	84.6	16.4	571.8	38.2	137.4	-0.46	A
HD987	1113	G8V	2621	19	502.6	116.8	2.5	393.6	6.4	103.1	-1.08	A
HD1466	1481	F8V	4400	19	135.8	39.6	7.4	189.8	17.6	55.9	-0.66	A
HD3221	2729	K4V	4014	5	4793.4	1794.3	68.6	3115.1	172.5	1447.8	-0.54	-
HD6569	5191	K1V	8	4	24.0	11.4	1.5	17.8	3.8	7.5	-1.49	A
HD7661	5938	K0V	1525	29	96.0	28.1	1.2	50.5	3.3	12.5	-1.42	A
HD10008	7576	K0V	4021	17	20.5	6.2	1.0	17.5	2.7	5.2	0.44	A
HD16765	12530	F7IV	926	27	173.0	47.2	11.0	402.9	27.9	93.1	-0.42	A
HD17925	13402	K1V	1470	40	113.6	30.5	1.1	58.7	3.1	17.4	-0.87	A
HD18599	13754	K2V	1055	16	115.9	38.9	1.5	54.3	3.9	17.6	-1.46	A
HD19668	14684	K0V	4402	20	143.1	33.2	1.8	91.9	4.7	26.0	-0.95	A
HD24916	18512	K4V	792	22	24.3	7.4	0.8	36.7	2.2	11.6	0.46	A
HD25457	18859	F6V	4089	78	187.2	49.5	3.3	345.4	7.7	60.2	-0.66	A
HD26923	19859	G0IV	4010	47	50.2	12.7	1.1	24.7	3.1	5.6	1.12	A
HD29391	21547	F0IV	3996	81	1476.1	326.2	28.4	2564.3	72.1	487.8	-	P
HD30447	22226	F3V	792	19	194.1	47.2	47.7	7048.7	106.6	1728.3	-	P
HD35650	25283	K6V	1195	13	48.3	15.3	1.2	43.6	3.0	12.3	-0.67	A
HD37572	26373	K0V	2826	34	347.1	75.4	1.7	223.6	4.4	52.8	-1.28	A
HD39060	27321	A6V	3702	5108	755.5	341.4	58.9					P
HD41593	28954	K0V	1194	15	69.5	19.8	1.1	59.4	2.9	16.7	-0.66	A
HD43989	30030	G0V	4433	17	819.0	238.6	15.6	743.7	34.3	197.6	-0.83	A
HD44627	30034	K1V	4892	23	670.6	177.7	3.2	428.6	8.1	110.9	-	A
HD45081	29964	K4V	4020	17	852.4	252.1	5.0	911.0	13.0	246.9	-	A
HD45270	30314	G1V	2827	19	137.4	51.8	3.1	193.3	8.4	59.2	-0.76	A
HD59967	36515	G3V	1065	25	65.3	19.7	1.4	41.6	3.6	10.5	-0.99	A
HD61005	36948	G8V	2369	33	186.5	48.8	2.5	127.4	6.3	32.7	-1.16	A
HD63608	37923	K0V	1069	36	80.7	22.2	1.1	49.1	3.0	11.7	-0.63	A
HD77825	44526	K2V	283	6	47.0	18.3	1.4	46.5	3.4	14.9	-1.09	A
HD82558	46816	K1V	1092	24	296.0	79.7	7.1	475.6	17.5	124.1	-0.43	A
HD89449	50564	F6IV	1227	28	129.9	41.4	4.3	351.6	9.1	113.6	-0.26	A
HD90905	51386	F5V	2551	24	125.6	40.8	1.9	187.7	5.0	49.0	-0.74	A
HD92945	52462	K1V	4533	38	182.3	40.5	1.5	86.2	3.9	23.8	-1.37	A
HD95086	53524	A8III	1532	103	1279.0	268.8	14.8	2594.0	36.3	511.1	-	P

Table A.2: Continued.

Stellar characteristics		Survey results.										$\langle \log R'_{\text{HK}} \rangle$	V	
Name HD/BD/CD	HIP ST (day)	TBL	N_m	RV (m s^{-1})		BVS (m s^{-1})		RV- BVS corr.	$\langle \text{FWHM} \rangle$	$\langle \log R'_{\text{HK}} \rangle$				
				A	rms	A	rms			A	rms			
HD95650	53985	4046	12	23.8	7.6	3.1	46.1	7.3	13.6	46.1	7.3	8.0	-4.330	-
HD99211	55705	3068	112	818.0	149.4	86.8	49704.0	214.7	5222.3	49704.0	214.7	183.4	-	P
HD102458	57524	2964	26	988.5	307.7	10.0	1358.4	23.8	431.7	1358.4	23.8	43.6	-3.994	A
HD103743	58241	1065	30	102.2	32.1	2.6	141.6	6.6	35.1	141.6	6.6	14.9	-4.308	A
HD105690	59315	2975	133	269.4	61.3	2.3	193.7	5.4	44.0	193.7	5.4	15.1	-4.276	A
HD106906	59960	1230	46	5290.4	1285.7	32.9	9949.8	83.3	2272.4	9949.8	83.3	74.0	-4.574	B
HD108767	60965	1201	18	47.9	12.4	0.7	25.3	2.0	7.7	25.3	2.0	8.2	-4.381	A
HD116434	65426	439	58	6273.2	1223.2	1235.6								P
HD118100	66252	720	10	534.7	155.6	6.4	139.5	15.6	43.0	139.5	15.6	16.5	-4.108	A
HD131399	72940	189	87	19478.2	6381.7	16.4	1287.6	39.3	237.0	1287.6	39.3	43.1	-	B
HD141943	-	2648	58	861.4	222.8	10.3	1169.7	25.3	269.6	1169.7	25.3	53.0	-4.025	A
HD146464	79958	51	5	872.1	352.1	5.0	546.2	12.3	220.6	546.2	12.3	25.8	-4.163	A
HD146624	79881	4762	335	232.7	39.8	29.2	70472.6	72.9	6163.4	70472.6	72.9	65.1	-	P
HD152555	82688	1135	22	225.0	64.8	6.1	283.2	15.9	69.9	283.2	15.9	26.3	-4.294	A
HD159492	86305	4751	90	612.4	124.9	20.8	2413.2	52.1	359.7	2413.2	52.1	79.4	-	P
HD164249	88399	1113	25	56.9	14.6	6.9	134.2	17.0	36.7	134.2	17.0	29.8	-4.765	A
HD169178	-	1123	19	354.7	135.7	1.8	85.6	4.7	25.0	85.6	4.7	10.7	-4.234	A
HD171488	91043	1111	18	2190.4	717.7	13.1	2249.5	33.2	680.4	2249.5	33.2	58.2	-3.988	A
HD172555	92024	2975	262	1883.8	329.6	70.6	94415.3	185.8	6148.5	94415.3	185.8	172.4	-	P
HD174429	92680	4572	42	3362.3	970.2	26.0	1167.7	60.0	320.7	1167.7	60.0	109.9	-	A
HD177171	93815	144	21	21233.2	5931.1	53.4							-4.047	B
HD181321	95149	3757	28	2610.2	683.2	3.9	244.0	9.6	59.1	244.0	9.6	19.5	-4.243	B
HD181327	95270	3496	56	63.1	16.3	3.8	156.8	9.0	30.6	156.8	9.0	28.8	-4.577	A
HD183414	96334	3097	68	247.9	63.6	2.4	214.0	6.2	58.3	214.0	6.2	16.0	-4.236	A
HD186704	97255	451	4	345.8	168.8	4.7	77.1	11.9	29.3	77.1	11.9	22.3	-4.308	T
HD188228	98495	4315	194	1398.7	319.2	150.2	211414.9	368.1	18294.0	211414.9	368.1	148.0	-	P
HD189245	98470	4285	46	646.2	119.4	21.0	5149.4	43.1	757.5	5149.4	43.1	104.2	-4.304	P
HD191089	99273	1025	26	107.1	22.8	15.7	300.0	37.3	78.4	300.0	37.3	57.0	-4.526	P
HD197481	102409	5619	55	667.6	144.0	3.2	470.1	8.0	101.2	470.1	8.0	16.2	-4.289	A
HD197890	102626	13	3	922.1	376.6	85.2	3975.6	217.1	1713.8	3975.6	217.1	216.2	-4.277	-
HD202917	105388	4438	20	436.1	124.6	5.0	438.1	12.4	134.8	438.1	12.4	23.0	-3.984	A
HD206860	107350	1332	22	122.1	35.8	2.8	180.9	6.7	51.4	180.9	6.7	16.1	-4.387	A
HD206893	107412	542	15	185.6	45.5	10.8	361.3	21.3	68.2	361.3	21.3	50.7	-4.630	P
HD207575	107947	2391	39	227.6	49.3	9.5	389.5	19.9	97.6	389.5	19.9	49.1	-4.332	P
HD213845	111449	4436	79	220.4	44.2	9.6	454.3	25.8	82.6	454.3	25.8	52.3	-4.703	P
HD215641	112491	1639	78	101.5	20.5	1.2	84.4	3.4	12.2	84.4	3.4	8.3	-4.460	A
HD216956	113368	4929	834	382.4	44.3	27.0	298.7	6.6	85.6	382.4	6.6	19.3	-	P
HD217343	113579	2727	26	276.6	96.9	2.7							-4.215	A

Table A.2: Continued.

Stellar characteristics			Survey results.									
Name	HIP	ST	TBL	N_m	RV		BVS		RV-BVS	$\langle \text{FWHM} \rangle$	$\langle \log R_{\text{HK}} \rangle$	V
HD/BD/CD		(day)			A	rms	A	rms	corr.			
					(m s^{-1})		(m s^{-1})					
HD217987	114046	M2V	5109	130	63.8	18.5	0.9	39.5	2.3	8.2	5.8	A
HD218396	114189	A5V	2727	124	3616.3	924.5	38.5	7376.0	95.5	2191.3	62.3	P
HD218860	114530	G8V	1137	18	137.1	36.2	2.1	82.8	5.4	18.6	11.7	A
HD221575	116258	K2V	869	16	45.7	12.2	1.4	33.4	3.7	12.0	8.8	A
HD223340	-	K1V	868	10	54.4	17.3	1.7	42.2	4.4	10.7	9.8	A
HD224228	118008	K2V	2815	31	35.4	8.8	1.0	31.5	2.8	7.5	7.8	A
-	6276	G9V	1201	20	95.6	27.3	1.6	91.0	4.2	27.6	9.4	A
-	116384	K7V	733	8	104.3	41.2	1.7	60.2	4.5	19.2	8.6	A
-	17157	K7V	1457	6	67.5	22.3	1.4	37.1	3.6	14.9	8.1	A
-	23309	M0V	4030	16	245.4	64.1	2.3	116.1	5.9	33.0	11.7	A
-	31878	K7V	435	11	84.3	31.6	1.6	48.3	4.1	16.1	8.5	A
-	36985	M2V	789	20	670.1	247.4	2.1	58.8	5.4	14.7	8.1	B
-	44722	K7V	90	4	8.0	3.4	1.5	10.7	3.8	4.0	7.6	A
-	46634	G5V	281	3	38.2	16.1	1.4	32.6	3.5	13.9	9.8	A
-	51317	M2V	4541	139	17.7	3.6	1.2	24.5	3.2	3.5	4.8	A
BD+20 2465	-	M5V	3983	40	63.5	16.1	1.2	33.6	3.1	6.5	6.7	A
CD-46 1064	-	K3V	1185	12	477.8	134.9	8.7	211.2	21.6	68.7	17.4	A

Appendix B: RV correction from the RV-BVS correlation

Solar to late-type stars present spots on their surfaces. These spots induce a quasi-periodic variations in the line profiles, which cause a signal in the RV and in the BVS. When the lines are resolved, there is at first order a correlation between the RV and the BVS (see Desort et al. (2007) for a detailed analysis)

To correct the RV signal induced by spots, we use Melo et al. (2007) method. It consists in correcting the RV from the linear regression of the RV vs BVS dataset. The new RV at a given date t is :

$$RV_{corr}(t) = RV(t) - (a * BVS(t) + b)$$

where a and b are the slope and the intercept of the best linear fit of the RV vs BVS dataset.

We present in Fig. B.1 an example of such correction for a star with $v \sin i = 31 \text{ km s}^{-1}$. The mean RV rms of 300 m s^{-1} are reduced to 60 m s^{-1} after correction. This method was used in precedent works that use SAFIR (Lagrange et al. 2013; Borgniet et al. 2017, 2019).

We present a star for which a significant offset due to the HARPS fiber change is present in the corrected RV in Fig. B.2. The initial mean RV rms are 36 m s^{-1} . After correction of the offset and of the RV-BVS correlation, the mean RV rms are 10 m s^{-1} .

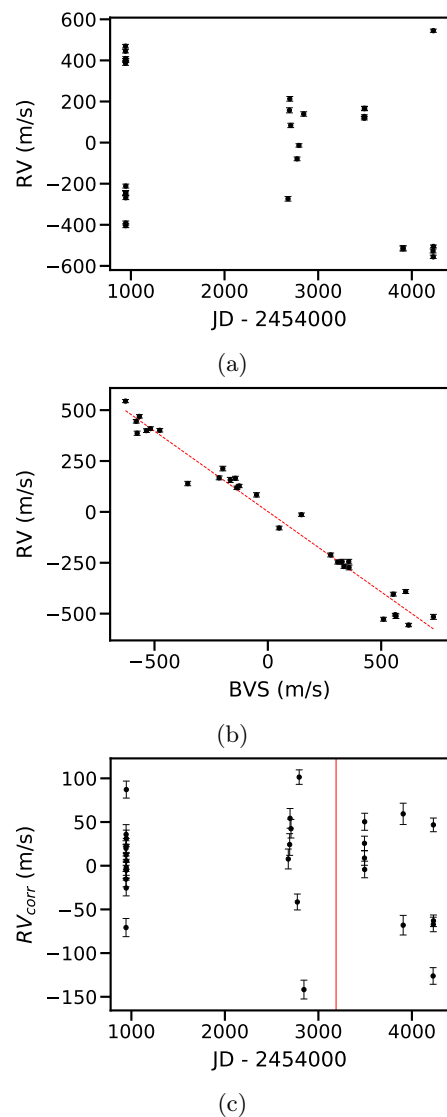


Fig. B.1: HD102458 RV jitter correction. a) RV time variations. b) RV vs BVS. The best linear fit is presented in red dashed line. c) RV corrected from the RV-BVS correlation. HARPS fiber change is shown with a vertical red line.

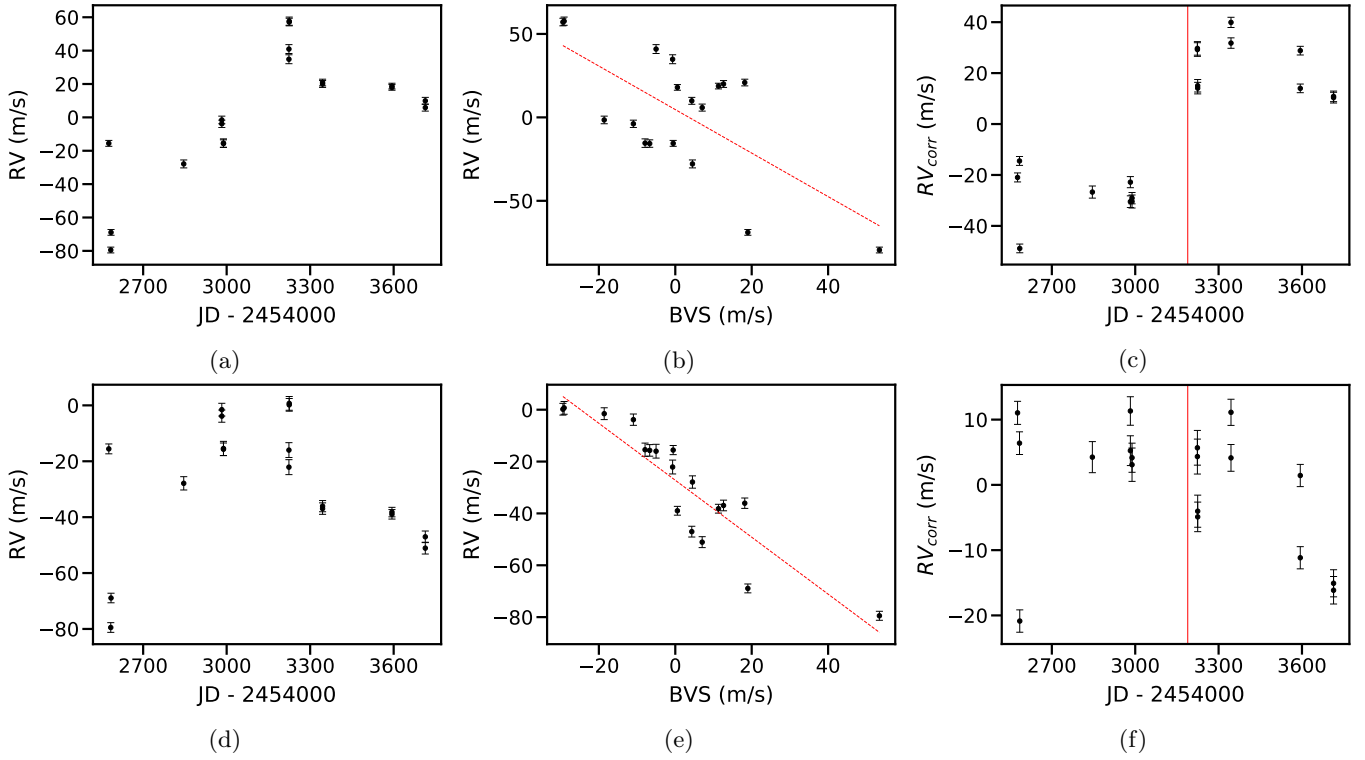


Fig. B.2: HD218860 jitter and offset correction. a) RV time variations. b) RV vs BVS . The best linear fit is presented in red dashed line. c) RV corrected from the RV-BVS correlation. HARPS fiber change is shown with a vertical red line. d) RV time variations corrected from the offset due to the HARPS fiber change. e) RV corrected from offset. vs BVS . The best linear fit is presented in red dashed line. f) RV corrected from offset, corrected from their correlation to the BVS. HARPS fiber change is shown with a vertical red line.